Title

Zirconium Carbide Mediates Coke-Resistant Methane Dry Reforming on Nickel-Zirconium Catalysts

Journal

Angewandte Chemie International Edition, 61(50)

ISSN

1433-7851

Authors

Haug, Leander
Thurner, Christoph
Bekheet, Maged F
et al.

Publication Date

2022-12-12

DOI

10.1002/anie.202213249

How to cite: *Angew. Chem. Int. Ed.* **2022,** *61,* e202213249
International Edition: doi.org/10.1002/anie.202213249
German Edition: doi.org/10.1002/ange.202213249

Methane Dry Reforming

Zirconium Carbide Mediates Coke-Resistant Methane Dry Reforming on Nickel-Zirconium Catalysts

*Leander Haug, Christoph Thurner, Maged F. Bekheet, Benjamin Bischoff, Aleksander Gurlo, Martin Kunz, Bernhard Sartory, Simon Penner, and Bernhard Klötzer**

Abstract: Graphitic deposits anti-segregate into Ni^0 nanoparticles to provide restored CH_4 adsorption sites and near-surface/dissolved C atoms, which migrate to the Ni^0/ZrO_2 interface and induce local Zr_xC_y formation. The resulting oxygen-deficient carbidic phase boundary sites assist in the kinetically enhanced CO_2 activation toward CO(g). This interface carbide mechanism allows for enhanced spillover of carbon to the ZrO_2 support, and represents an alternative catalyst regeneration pathway with respect to the reverse oxygen spillover on Ni-$CeZr_xO_y$ catalysts. It is therefore rather likely on supports with limited oxygen storage/exchange kinetics but significant carbothermal reducibility.

Introduction

Dry reforming of methane (DRM) allows converting the climate-harming greenhouse gases methane and carbon dioxide to CO-rich syngas at an ideal stoichiometry of $CH_4 + CO_2 \rightarrow 2H_2 + 2CO$. To approach this 1:1 ratio is rather useful for subsequent carbonylation or hydroformylation processes.[1] Practical problems of DRM are associated with further loss of H_2-selectivity due to the water-gas-shift equilibrium, especially at elevated pressures,[2] and with irreversible coking phenomena, especially on the less costly Ni- and Co-based catalysts.[3–6] Countermeasures against coking involve the addition of steam, leading to an increased H_2:CO ratio. Technically, endothermic hybrid dry-steam reforming ("bi-reforming"),[7] and autothermal tri-reforming[8] lead to more suitable syngas ratios for the synthesis of e.g. renewable fuels. For these applications, requirements such as structural stability and tuned catalyst composition must be met for improving carbon gasification activity. Long-term stable industrial catalysts allowing for coke-depleted operation under conditions with a low steam/carbon ratio are already available, and are e.g. based on NiMg spinels.[9,10]

Nevertheless, it appears worthwhile to further study the most challenging steam-free DRM case with $CO_2:CH_4 = 1:1$ feed at the fundamental atomistic level, serving as a benchmark reaction to identify and develop knowledge-based strategies against irreversible coking phenomena.

Frequently, anti-coking strategies make use of graphene/graphite and nanofilament-suppressing dopants of the metallic component Ni^0, such as Cu^0.[11] Selective blocking of the step edges of nickel crystallites with sulfur (SPARG process)[12,13] or the use of gold as a catalyst dopant[14] are typical examples. From a mechanistic viewpoint, this approach is inherently accompanied by lowered methane activation rates, and thus, lowered activities.[6] Moreover, this approach cannot exclude partially irreversible coking, as it may occur at a lowered rate, too.

A logical complementary strategy should therefore focus on optimized conversion both of methane and of already deposited carbon species toward CO_2-reactive forms of carbon, in turn enhancing the route to CO. Some carbides of the group V and VI transition metals are considered as active phases, due to their noble metal-like electronic structure facilitating reactant activation. Enhanced coking stability is assigned to a balanced combination of carbophobic properties suppressing the formation of too strongly bonded (e.g. unreactive graphitic) carbon species, and moderate oxophilicity for controlled CO_2 activation towards reactive oxygen species at the surface. If the oxygen affinity is too high, as with the group V metals, both surface and bulk carbide phase stability are hampered. Group VI carbides, especially Mo_2C and WC, are more stable but still affected by surface-near corrosion under CO_2-rich conditions. They can be further activated and stabilized by the addition of metals promoting re-carburization, e.g. Co.[15,16]

A related approach is to enhance the surface oxophilicity of a metallic component, along with promoting more

[*] L. Haug, C. Thurner, Dr. S. Penner, Prof. B. Klötzer
Institute of Physical Chemistry, University of Innsbruck
Innrain 52 c, 6020 Innsbruck (Austria)
E-mail: Bernhard.Kloetzer@uibk.ac.at
Dr. M. F. Bekheet, B. Bischoff, Prof. A. Gurlo
Fachgebiet Keramische Werkstoffe, Institut für Werkstoffwissenschaften und -technologien, Technische Universität Berlin, Straße des 17. Juni 135, 10623 Berlin (Germany)
Dr. M. Kunz
Advanced Light Source
Lawrence Berkeley National Laboratory
Berkeley, CA 94720 (USA)
B. Sartory
Materials Center Leoben Forschung GmbH
Roseggerstrasse 12, 8700 Leoben (Austria)

reactive and less refractory forms of carbon, e.g. using Fe^0 alloying of Ni^0.[17] On MnO-supported Ni, particular non-graphitic surface carbon species exhibit enhanced reactivity toward CO_2.[18–20]

As a matter of fact, it is the progressive poisoning of active sites by continuously deposited unreactive (spectator) species, which causes irreversible catalyst deactivation over time—but if active sites can be designed in a self-regenerating environment, a certain remaining fraction of unreactive or only slowly reacting coke will eventually be little harmful to the overall catalyst performance. Therefore, we focussed on the distinction of reactive *intermediate* vs. unreactive *spectator* carbon species by in situ techniques, and on promotional effects to *re-mobilize* already existing carbon deposits in the present study.

Our previous in situ Near-Ambient Pressure X-Ray Photoelectron Spectroscopy (NAP-XPS) studies on intermetallic PdZr catalyst precursors[21,22] provided evidence that deposited $C_{graphite}$ can be re-activated toward dissolved atomic C-species in nanoparticulate Pd^0, and finally oxidized to CO at the redox-active Pd^0-ZrO_2 phase boundary (in the following abbreviated "PB"). On this basis, we proposed that improved subsurface- and bulk C-diffusivity of the metallic component co-operates with an improved level of metal-oxide bifunctionality. Based on the results for pure Pd, we suspected a related de-coking mechanism for NiPd/ZrO_2 catalysts. Thus, the next logical step is first to clarify the role of the analogously prepared Ni^0-ZrO_2 PB using in situ NAP-XPS.

In contrast to clean Pd, both pure and alloyed Ni surfaces are in principle capable of activating both CH_4 and CO_2,[23,24] which is particularly important if inert supports with respect to CO_2 activation are used. An additional, PB-related type of bifunctionality can be expected, if an already efficient CH_4 activator such as Ni is combined with a support being capable of CO_2 activation. In this case, subsequent CO product formation is not necessarily limited to the Ni surface itself, but can also take place at Ni^0—support interface sites. Depending on the intrinsic state of activity of the Ni surface, the enhanced abundance and activity of interfacial sites can thus contribute to enhanced dry reforming activity and optimized de-coking properties. In view of this "structure sensitivity" also of Ni-based catalysts, empirical development of catalyst preparation and -activation must logically aim in optimized interface dimensions to a support with good CO_2 activation kinetics. An enhanced density of interfacial Ni-support sites vs. Ni surface sites can be achieved by lowering the Ni^0 particle size, and has been shown to enhance the coking stability and lower the propensity for the formation of filamentous carbon.[25] Critical parameters determining CO_2 activation at the PB encompass support reducibility, basicity, and reactivity of oxygen vacancies toward CO_2.[9,26] Some of the most recently developed industrial bi-reforming catalysts are designed to utilize self-regenerating principles.[9,10]

Due to their structural heterogeneity and the limited applicability of surface-sensitive in situ spectroscopies such as NAP-XPS, technical powder catalysts usually do not allow to extract unambiguous evidence for the catalytic role of the metal-oxide PB. The use of conductive bimetallic substrates, on which an active layer forms under reaction conditions via oxidative segregation, both allows to circumvent conductivity problems and to provide a quasi-2D region of spectral observation. Thus, a bulk bimetallic Ni_xZr_y model catalyst approach toward active PB sites was employed. The in situ activation of intermetallic precursors is a highly efficient way to generate a large amount of PB sites.[22,27] We used a combination of in situ X-Ray Diffraction (XRD) and in situ NAP-XPS analysis to characterize both the bulk-related phase changes and the active surface/interface in a realistic DRM atmosphere.

Results and Discussion

Details of the preparation and structural characterization of the used bulk-intermetallic $Ni_x{}^0Zr_y{}^0$ sample with an initially dominant contribution of the Ni_5Zr phase—in the following denoted as NiZr51—are given in the experimental section of the Supporting Information. The surface morphology of the as-prepared NiZr51 sample was characterized by ex situ Scanning Electron Microscopy (SEM, Setup 5 in Supporting Information) and is depicted in Figure 1A.

Due to ambient air contact, near-surface corrosion induces the formation of small (<10 nm) Ni nanoparticles supported by a thin ZrO_2 top layer. After transfer to an ultrahigh vacuum (UHV) chamber with an attached high-pressure batch reactor (Supporting Information, Setup 1), the chemical surface composition of the NiZr51 sample was characterized after a sputter-anneal cycle by ex situ XPS, representing the surface state of the catalyst directly before temperature-programmed DRM catalysis (Figure S1, Supporting Information). The coexistence of intermetallic Zr^0, sub-oxidic ZrO_x and a small contribution of Zr^{+4} species, along with exclusive Ni^0 species, indicates incomplete removal and/or partial reduction of ambient-induced Zr^{+4} species by sputtering.

To identify bulk-structural changes toward the operando state, in situ X-ray diffractograms of NiZr51 were recorded during temperature-programmed reaction under 1:1 DRM conditions. Figure 1B is derived from the respective XRD series shown in Figure S2 (for details and exact mass fraction data see section S2, Supporting Information), and reveals that the initial phase composition of Ni_5Zr and Ni^0 persists to $\approx 350\,^{\circ}C$, followed by partial decomposition of Ni_5Zr towards tetragonal (t-)ZrO_2 and additional Ni^0. The subsequent transformation of t-ZrO_2 to monoclinic (m-)ZrO_2 is associated with slower Ni_5Zr decomposition. During cooling and re-heating in pure CO_2, no further phase changes occurred. Figure S2, Supporting Information, further reveals that neither crystalline $C_{graphite}$ nor carbide bulk phases, nor irreversible lattice expansion of Ni^0 due to dissolved carbon were XRD-detectable, in contrast to related studies on Ni/MnO.[18–20]

Figure 1C shows an ex situ SEM image of the coked NiZr51 catalyst after DRM up to $800\,^{\circ}C$ and cooling under UHV conditions. A rather heterogeneous morphology and size distribution of the Ni domains is visible, giving the

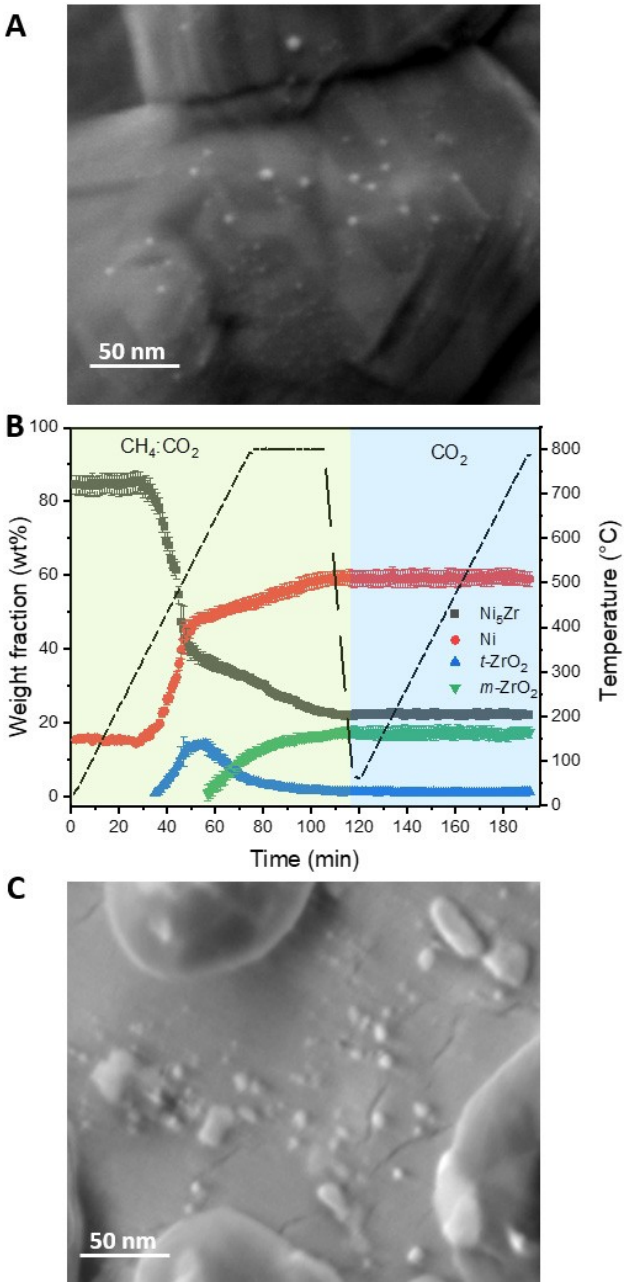

Figure 1. A) SEM image of the as-grown bulk-intermetallic NiZr51 catalyst. B) Development of mass fractions of crystalline phases within NiZr51 from 25 °C to 800 °C under DRM conditions (CH_4:CO_2 = 1:1, 40 mL min^{-1}, total pressure 1 bar, heating rate 10 K min^{-1}) as derived from Rietveld analysis of the in situ XR diffractograms shown in Figure S2, Supporting Information. C) Ex situ SEM image of the catalyst in its coked active state after DRM.

impression of a bimodal state. Nanoparticles in the 10 nm range, some larger, some even smaller, contrast with very large Ni islands between ≈100 and ≈300 nm. Figure S3, Supporting Information, shows additional topographic images and the respective Energy Dispersive X-Ray Spectroscopy (EDX) scans, revealing that especially the large Ni domains are covered by considerable amounts of carbon, whereas the support regions with the Ni nanoparticles appear less affected.

Quantitative temperature-programmed DRM experiments on the NiZr51 sample were performed in an UHV-compatible high-temperature recirculating batch reactor (Supporting Information: Setup 1), and compared to the activity of a clean Ni metal foil. The respective conversion and turnover number (TON) data on NiZr51 are shown in Figure 2A, revealing an exponential increase in the CO_2 conversion above ≈480 °C. This can be rationalized by the Ni^0 XRD intensity results of Figure 1B. Accumulation of uncoked, nano-dispersed Ni^0 in contact with segregated ZrO_2 until 480 °C is held responsible for this earlier reaction onset. Full conversion is approached during the isothermal period at 800 °C. Selectivity-wise, the CO:H_2 product ratio remained close to 1:1 at any temperature, and accordingly, CO_2 consumption to CO formation was close to 1:2. In contrast, the pure Ni foil showed zero activity at above 480 °C and a rapid reaction onset around 640 °C, as indicated

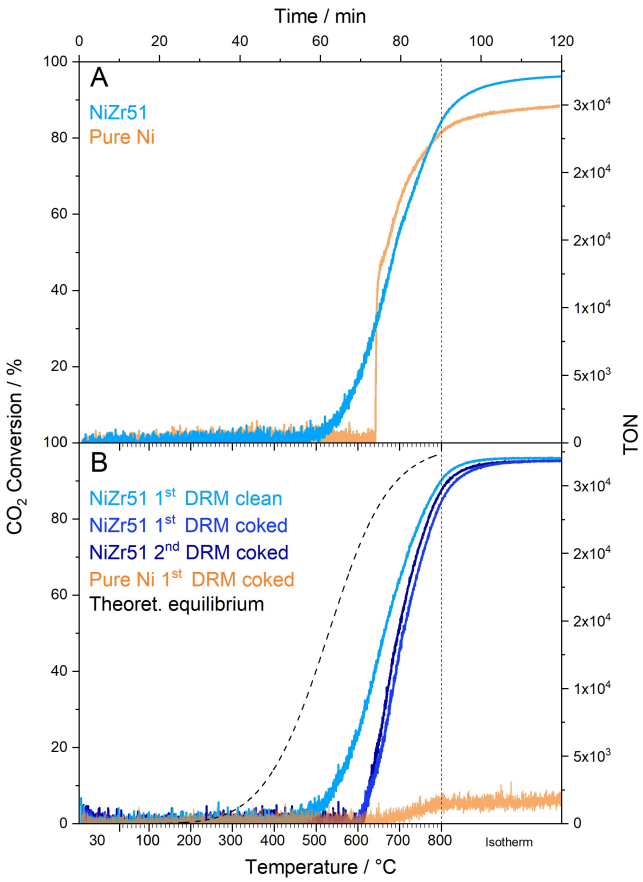

Figure 2. A) Temperature-programmed CO_2 conversion/TON DRM profile on fresh NiZr51 plotted versus the respective data measured on a clean metallic Ni foil. B) Repeated DRM experiments on the coked catalysts resulting from the initial DRM runs. Reaction conditions: 50 mbar CH_4, 50 mbar CO_2, 977 mbar He; linear temperature ramp (10 K min^{-1}) up to 800 °C, followed by isothermal reaction for 30 min. The dashed line represents the calculated temperature-dependent equilibrium conversion of the used reaction mixture toward a stoichiometric 1:1 H_2:CO product ratio (details of calculation see Supporting Information, Setup 1).

by the step-wise increase of conversion up to >40 %. The quenching experiments of Figure S4 (Supporting Information) reveal that this effect is associated with the sudden breakdown of a passivating NiO layer that was formed on the catalyst surface in the DRM atmosphere between room temperature and ≈600 °C. Panel B of Figure 2 exemplifies the fundamental reactivity differences between the spent states of NiZr51 and bulk Ni after the first DRM cycle. Whereas the latter remains largely deactivated, the NiZr51 sample exhibits a reproducible shift of the onset temperature to ≈600 °C in the subsequent two cycles, as compared to ≈480 °C upon starting from fresh NiZr51, but the further course of all subsequent conversion profiles approaches the performance of the first cycle.

In order to clarify the origin of the extremely improved catalytic stability in relation to bulk Ni, the coking status and the reactivity of carbonaceous deposits toward CO_2 were tested on the DRM-pre-treated NiZr51 catalyst (i.e., in the state after the "2nd DRM coked" cycle of Figure 2B/ Figure S1), using in situ NAP-XPS. This experimental order was inevitable to study the fully coked state, as the gas phase conditions in the NAP-XPS chamber did not suffice to deposit enough $C_{graphite}$, mainly due to the too low pressure and gas temperature of CH_4 (for details see Supporting Information, Setup 2). The topmost spectra in Figure 3, taken at 800 °C *in vacuo* before exposure to CO_2, provide clear evidence of a considerable carbidic Zr_xC_y contribution (details of XP spectral assignment and analysis see Supporting Information), which was formed during heating of the coked catalyst in vacuum. Despite the initial presence of a large amount of $C_{graphite}$, Zr_xC_y species were neither detectable in the ex situ room temperature XP spectrum of Figure S1, Supporting Information, nor in the spectrum after transfer to the NAP-XPS system before heating.

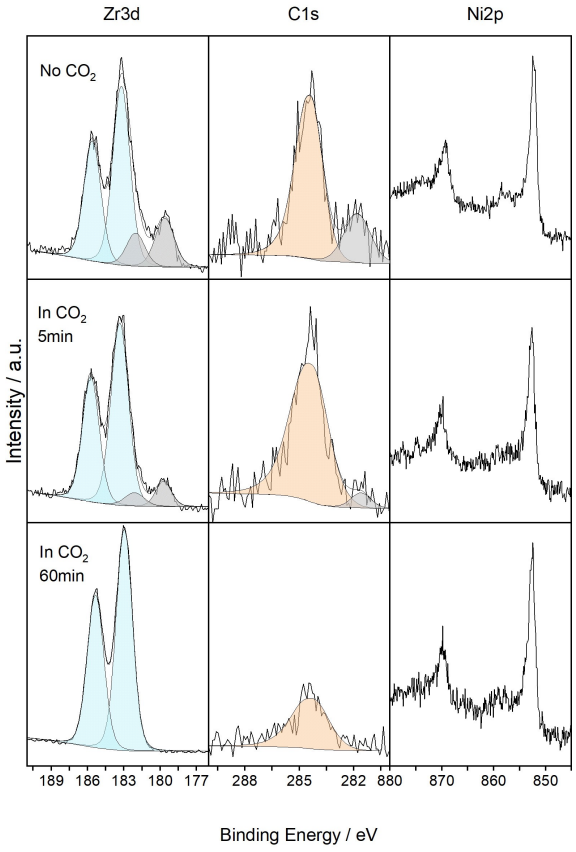

Figure 3. In situ Zr3d, C1s and Ni2p NAP-XP spectra recorded on spent NiZr51 after the "2nd DRM coked" cycle. Top panels: spectra at 800 °C in vacuum. Middle and lower panels: spectra at 800 °C in 0.2 mbar pure CO_2 recorded after the indicated times.

We emphasize that $C_{graphite}$ is mainly accumulated on the Ni^0 surface area, as evidenced by the Ni2p intensity trends of Figure S1 and the EDX-maps of Figure S3, Supporting Information. Therefore, the occurrence of surface-near Zr_xC_y species suggests a thermally induced re-distribution mechanism of carbon from the $C_{graphite}$ deposits on Ni^0 toward the surrounding ZrO_2 support, causing its local carbothermal reduction toward Zr_xC_y. The fact that the in situ XRD data do not support the formation of crystalline Zr bulk carbide phases may be explained by a limited total amount of surface-near and/or interfacial Zr_xC_y, along with an unknown contribution of amorphous species.

The solid-state synthesis reaction of crystalline bulk ZrC by carbothermal reduction of pure ZrO_2 is moderately endothermic ($ZrO_2(s)+3C(s)\rightarrow ZrC(s)+2CO(g)$, $\Delta H^0_{298}\approx +46\,kJ\,mol^{-1}$) and proceeds upon heating between 1500 °C and 1800 °C[28] via direct graphite-zirconia interaction. Therefore, it appears reasonable that the formation of the interfacial Zr_xC_y species from $C_{graphite}$ on Ni^0 and ZrO_x at the metal-oxide PB is endothermic and cannot proceed without heating. To explain the strongly reduced formation temperatures on activated NiZr51, we suggest a catalytic role of Ni^0 for Zr_xC_y formation, as it is capable of re-dissolving $C_{graphite}$ at $T>650$ °C and of transporting reactive C atoms through the bulk and/or along the surface toward the PB.[16–18,29,30]

The most interesting result concerns the relative reactivities of the Zr_xC_y vs. $C_{graphite}$ species toward CO_2. As shown in the middle and lower panels of Figure 3, the Zr_xC_y component decreases at a much higher rate than the graphitic one. Obviously, Zr_xC_y is more reactive than $C_{graphite}$ with respect to the clean-off reaction in pure CO_2. At 800 °C, it takes around 5 min to reduce the Zr_xC_y signals by more than 50 %, but around 60 min to achieve a >50 % decrease for graphitic C, while Zr_xC_y is already gone.

The results of Figure 3, which are only accessible by in situ XP spectroscopy under close-to-real conditions, suggest that Zr_xC_y plays the role of a reactive intermediate in between $C_{graphite}$ and CO(g). The fact that at least a part of the thermal C redistribution process $C_{graphite}\rightarrow Zr_xC_y$ proceeds at a much lower rate than that of the final Zr_xC_y clean-off step, simplified as $ZrC(s)+3CO_2(g)\rightarrow ZrO_2(s)+4CO(g)$, may be assigned to the presence of the large, coke-deactivated Ni^0 domains observed on NiZr51 (Figure 1C and Figure S3, Supporting Information). This appears plausible, as the equally coke-covered pure Ni^0 foil (Figure 2B, after the 1st DRM cycle) experiences almost irreversible deactivation, which suggests that the direct oxidation process $C_{graphite}+CO_2(g)\rightarrow 2CO(g)$ on the Ni^0 surface is very inefficient. Nevertheless, the presence of the Ni^0/ZrO_2 PB on NiZr51 allows for slow, yet almost complete de-coking even of the

largest Ni^0 domains with CO_2, in contrast to pure bulk Ni^0. Figure S5, Supporting Information, shows the complementary kinetic data of CO_2 titration of $C_{graphite}$ on coked Ni foil vs. NiZr51, along with the respective pre- and post-titration C1s spectra. Clearly, $C_{graphite}$-covered bulk Ni^0 exhibits almost zero reactivity toward CO_2(g) at 800 °C and cannot be de-coked on a reasonable timescale, whereas coked NiZr51 can be cleaned off to a major extent—although in part slowly—highlighting the decisive mechanistic role of the PB. Vice versa, the pure ZrO_2 support without Ni^0 contact is also hardly active, as shown in Figure S6, Supporting Information. Its low, but measurable intrinsic reactivity at T > 600 °C is not affected by coking, carbidization or any other spectroscopic alterations, but cannot explain the much higher catalytic activity of the Ni/ZrO_2 PB system.

Here, at the latest, the question arises which form of Ni^0 allows for the most efficient decoking and CO formation route and thus constitutes the most active species. As activated NiZr51 features a quasi-bimodal catalyst state, the abundant Ni nanoparticles with a large support PB contribution represent the most likely candidates, as they feature a combination of enhanced carbon solubility, short diffusion pathways to the surrounding PB and an enhanced ratio of PB vs. metallic surface sites.

To prove the dominant role of the active Ni nanoparticle —ZrO_2 PB, analogous catalytic and in situ spectroscopic measurements were performed on small Ni nanoparticles supported on a monoclinic ZrO_2 powder substrate. The respective results are provided in Figures S7 and S8, Supporting Information. The wet-impregnated Ni10Zr90 (5 % Ni^0/ZrO_2) catalyst shown in Figure S7, panel A exhibits evenly distributed Ni particles with ≈7 nm average size and was tested in temperature-programmed DRM experiments in Setup 4 (dedicated to powder catalyst measurements, see experimental section, Supporting Information). Thereby, the conditions used for the NiZr51 intermetallic sample in Setup 1 were closely simulated. The resulting "DRM I″ CO_2 conversion curve shown in Figure S7, panel C strongly resembles that of the "1st DRM clean" run on NiZr51 (Figure 2B, onset at ≈500 °C, ≈90 % conversion at 800 °C). In analogy to the "1st and 2nd DRM coked" conversion traces in Figure 2B, the supported Ni10Zr90 catalyst exhibited some deactivation in the second cycle ("DRM II" in Figure S7, panel C). The cause of this deactivation, pronounced Ni particle sintering to sizes between ≈10 and ≈30 nm, is obvious from the post-DRM SEM image in Figure S7, panel B. Further DRM cycles (not shown) caused no additional Ni sintering, and "DRM II" is thus representative for the reproducible performance of the coked Ni10Zr90 catalyst state, which in turn strongly resembles that of the "1st and 2nd DRM coked" runs on NiZr51 (Figure 2B, onset at ≈600 °C, 70–80 % conversion at 800 °C).

Based on this clear proof of well-comparable catalytic performance, in situ NAP-XPS measurements of the coked state of Ni10Zr90 were performed in pure CO_2, in close analogy to the CO_2-reactivity experiments on coked NiZr51 shown in Figure 3. Figure S8, Supporting Information, reveals that the main difference observed in direct comparison of NiZr51 and Ni10Zr90 is the strongly enhanced rate of carbon clean-off on the latter. The absence of the very large, bulk-like Ni^0 domains gives rise to almost complete de-coking within 10 minutes, even at 700 °C instead of 800 °C. Experimentally, it was not possible to distinguish the individual rates of Zr_xC_y and $C_{graphite}$ conversion, as both processes occurred almost quantitatively (except some tiny traces of residual $C_{graphite}$) on the shortest possible timescale for obtaining reasonable XPS spectra. We regard this as a clear proof that the thermal C redistribution process $C_{graphite} \rightarrow Zr_xC_y$, and thus the entire DRM process, proceeds along the same mechanistic route as on NiZr51, albeit at a much higher rate on the Ni nanoparticles, which can explain the high DRM activity observed on either catalyst type. The fact that no surface-near accumulation of carbon could be observed during any in situ NAP-XPS experiments in CH_4—CO_2 mixtures, can be explained on the basis of a short lifetime in the presence of CO_2, along with the aforementioned slow deposition of carbon due to the low sticking coefficient of "cold" CH_4.[31,32]

Conclusion

The synopsis of these pieces of experimental evidence allows us to deduce the picture of a bifunctional PB mechanism, which is visualized in Scheme 1: at sufficiently high temperatures at and beyond 700 °C, $C_{graphite}$ deposits on Ni, which

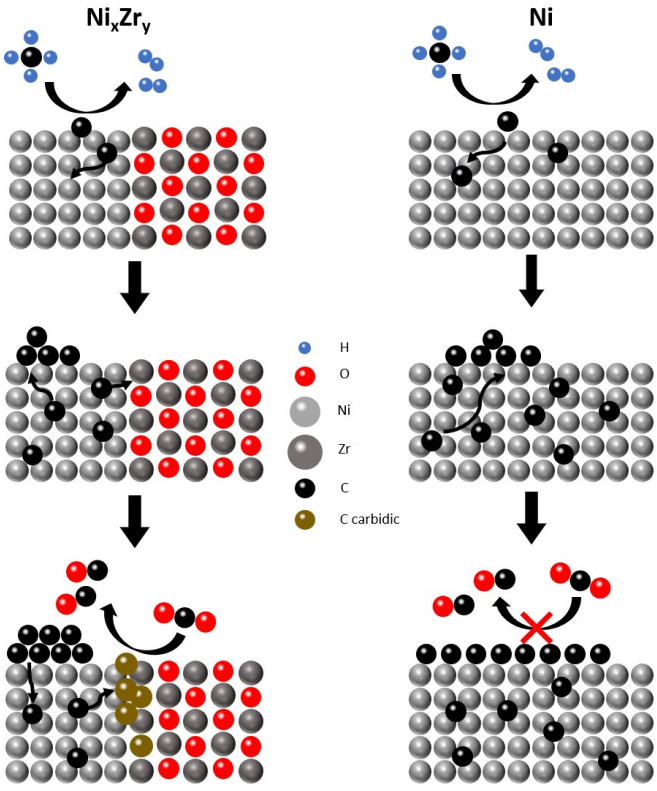

Scheme 1. Proposed DRM mechanism leading to enhanced CO-formation at the Ni/ZrO_2 interface.

originate from methane decomposition, are mobilized toward endothermic Zr_xC_y formation, specifically in the catchment area around the coked Ni^0 domains. The rate of this "carbon spillover" strongly depends on the particle size-dependent C diffusion lengths inside/on Ni and the associated PB dimensions, which are both favored for small Ni^0 nanoparticles with enhanced metal-support interaction. The spillover creates a permanently active, carbophobic and oxophilic (thus, coke-protected) interfacial zone, where CO_2 can react with Zr_xC_y toward CO through a lowered kinetic barrier as compared to the direct reaction with $C_{graphite}$ on bulk Ni^0.

This "interface carbide mechanism" accelerates the inverse Boudouard reaction, which is the dominant de-coking process at higher temperatures, especially around the Ni^0 nanoparticles. In consequence, active zones within the entire catalyst surface area are permanently re-established, despite the accumulation of a large amount of Ni-surface blocking graphitic deposits, which are particulariy unreactive on the large Ni^0 domains due to long-range C-diffusion limitations. As these deposits can slowly grow and shrink without harming the carbidic active zones, even strongly coked states of the catalyst retain reproducible activity after many catalytic cycles, provided that the dispersion of the nanoparticles remains stable over time.

Material-wise, the in situ decomposition of Ni-rich intermetallic Ni_xZr_y pre-catalysts gives rise to quasi-bimodal Ni^0/ZrO_2 interface systems with optimized PB dimensions due to the presence of finely dispersed, relatively sinter-stable Ni^0 nano-islands/particles. Obviously, only the latter aspect is helpful for establishing coking-tolerant Ni-based DRM catalysts. This contrasts with pure bulk Ni metal, which becomes initially passivated by CO_2-induced surface oxidation, rendering it carbophilic only for a single catalytic cycle. Once metallic and fully coke-covered (right side in Scheme 1), it remains largely deactivated with respect to the direct $C_{graphite}$ clean-off reaction with CO_2.

Regarding the detailed C-spillover/conversion mechanism, we suggest that $C_{graphite}$ deposits anti-segregate into the Ni^0 particles/domains to provide both "recycled" CH_4 adsorption sites on Ni^0 and local diffusion of adsorbed and dissolved carbon atoms toward the ZrO_2 interface, where they get trapped. A direct methane-activating role of the in situ formed Zr_xC_y domains cannot be excluded, but a major contribution to the total methane conversion appears unlikely in view of their short lifetime and low abundance. As e.g. pure bulk Mo_2C exhibits even poorer activity than a pure ZrO_2 support,[16] a dominant catalytic role of the even less stable Zr_xC_y, beyond its CO_2-consuming role in the PB mechanism, appears highly unlikely.

Therefore, the anti-segregation process of $C_{graphite}$, starting at $\approx 600\,^{\circ}C$[33] and becoming sufficiently fast at $\approx 700\,^{\circ}C$, is critical for maintaining both the Zr_xC_y (re-)formation and the re-formation of CH_4 adsorption sites on Ni^0. The absence of this type of carbon sink can explain e.g. the larger C-supersaturation of Ni^0 particles supported on MnO.[17,18] Carbidic and/or other oxophilic oxygen-deficient Zr sites then assist in reductive CO_2 activation toward the first CO(g) molecule. Thereby Zr_xC_y becomes (partially) re-oxidized, and the full catalytic cycle is completed via the release of the second CO(g) molecule, likely formed at an intermediate "oxycarbidic" site.

Recently reported attempts to control coking of highly dispersed Ni^0 by specifically redox-active supports such as $CeZr_xO_y$[34,35] rather utilize the oxygen storage capacity of the support and the associated reverse spillover of oxygen to Ni, promoting both local CO formation and de-coking. In this work, we were able to identify an alternative catalyst regeneration pathway through an interface carbide mechanism, which is rather likely on supports with limited oxygen exchange kinetics but significant carbothermal reducibility.

The mechanistic scenario of Scheme 1 provides a solid basis for the directional promotion of microkinetic steps leading both to enhanced activity and improved control of carbon chemistry during DRM. Accordingly, improved Ni^0/ZrO_2 catalyst designs should be based on, and/or developed via preparation routes aiming both in optimized Ni^0 dispersion and long-term stabilization with respect to sintering. Our "first try", the conventional wet-impregnated Ni10Zr90 catalyst system, already showed the basic validity of this concept, but suffered from pronounced particle sintering already after the first DRM cycle.

In summary, the general implications for knowledge-based DRM catalyst synthesis, at least if C-dissolving metals such as Ni and Pd are involved, are: (1) optimization and high-temperature stabilization of PB dimensions to, and CO_2 activation properties of a support with active carbon chemistry; (2) adjustment of (bi)metal particle size to achieve continuous and fast C_{bulk} depletion in metallic regions with the largest distance to the PB; (3) use of (bi)metallic catalysts with optimized $C_{graphite}$ dissolution properties, but at the same time suppressed nucleation- and growth kinetics of $C_{graphite}$ species; (4) high abundance and reactivity of mobile C atoms at the interface, achievable via optimized CH_4 adsorption/ sticking at the C-free metallic surface and fast bulk/surface diffusion to not too strongly C-binding sites within an "carbon-oxygen interdiffusion zone" close to the PB. As shown in this work, the use of Ni-rich intermetallic precursors such as NiZr51 or conventional wet-impregnated Ni/ZrO_2 catalysts can only partially match these criteria.

Acknowledgements

The Austrian Promotion Agency (FFG) is acknowledged for funding of the NAP-XPS instrument through F&E infrastructure project 870523 "XPS In situ and Operando Investigations of Functional Materials". Leander Haug acknowledges funding through FFG project 870523. Christoph Thurner acknowledges a PhD position via the doctoral program "reactivity and catalysis" of the University of Innsbruck. The authors thank the Advanced Light Source, which is supported by the Director, Office of Science, Office of Basic Energy Sciences, of the U.S. Department of Energy under Contract No. DE-AC02-05CH11231, and where the in situ XRD measurements were conducted at beamline 12.2.2

in the framework of the proposals AP (ALS-08408) and GUP (ALS-10533).

Conflict of Interest

The authors declare no conflict of interest.

Data Availability Statement

The data that support the findings of this study are available from the corresponding author upon reasonable request.

Keywords: Carbon Spillover · Methane Dry Reforming · Near Ambient Pressure XPS · NiZr Intermetallic Catalyst · Zirconium Carbide

[1] M. Gupta, J. J. Spivey in *New and Future Developments in Catalysis*, Elsevier, Amsterdam, **2013**, pp. 87–126.
[2] S. T. Oyama, P. Hacarlioglu, Y. Gu, D. Lee, *Int. J. Hydrogen Energy* **2012**, *37*, 10444.
[3] A. Wolfbeisser, O. Sophiphun, J. Bernardi, J. Wittayakun, K. Föttinger, G. Rupprechter, *Catal. Today* **2016**, *277*, 234.
[4] A. W. Budiman, S.-H. Song, T.-S. Chang, C.-H. Shin, M.-J. Choi, *Catal. Surv. Asia* **2012**, *16*, 183.
[5] L. Wu, X. Xie, H. Ren, X. Gao, *Mater. Today Proc.* **2021**, *42*, 153.
[6] E. Schwab, A. Milanov, S. A. Schunk, A. Behrens, N. Schödel, *Chem. Ing. Tech.* **2015**, *87*, 347.
[7] G. A. Olah, A. Goeppert, M. Czaun, G. K. S. Prakash, *J. Am. Chem. Soc.* **2013**, *135*, 648.
[8] C. Song, W. Pan, *Catal. Today* **2004**, *98*, 463.
[9] K. Wittich, M. Krämer, N. Bottke, S. A. Schunk, *ChemCatChem* **2020**, *12*, 2130.
[10] V. Lanver, R. M. D. Kaufmann, S. Altwasser, EP3574994 (A1), **2018**.
[11] K. Song, M. Lu, S. Xu, C. Chen, Y. Zhan, D. Li, C. Au, L. Jiang, K. Tomishige, *Appl. Catal. B* **2018**, *239*, 324.
[12] J. R. Rostrup-Nielsen, J. Sehested, J. K. Nørskov in *Advances in Catalysis*, Elsevier, Amsterdam, **2002**, pp. 65–139.
[13] P. M. Mortensen, I. Dybkjær, *Appl. Catal. A* **2015**, *495*, 141.
[14] S. Palma, L. F. Bobadilla, A. Corrales, S. Ivanova, F. Romero-Sarria, M. A. Centeno, J. A. Odriozola, *Appl. Catal. B* **2014**, *144*, 846.
[15] A. J. Brungs, A. P. York, M. L. Green, *Catal. Lett.* **1999**, *57*, 65.
[16] X. Du, L. J. France, V. L. Kuznetsov, T. Xiao, P. P. Edwards, H. AlMegren, A. Bagabas, *Appl Petrochem Res* **2014**, *4*, 137.
[17] T. Zhang, Z. Liu, Y.-A. Zhu, Z. Liu, Z. Sui, K. Zhu, X. Zhou, *Appl. Catal. B* **2020**, *264*, 118497.
[18] A. Gili de Villasante, *High-temperature separation and activation of carbon dioxide by dual-phase membranes and nickel catalysts*, Technische Universität Berlin, **2020**.
[19] A. Gili, L. Schlicker, M. F. Bekheet, O. Görke, D. Kober, U. Simon, P. Littlewood, R. Schomäcker, A. Doran, D. Gaissmaier et al., *ACS Catal.* **2019**, *9*, 6999.
[20] A. Gili, L. Schlicker, M. F. Bekheet, O. Görke, S. Penner, M. Grünbacher, T. Götsch, P. Littlewood, T. J. Marks, P. C. Stair et al., *ACS Catal.* **2018**, *8*, 8739.
[21] N. Köpfle, T. Götsch, M. Grünbacher, E. A. Carbonio, M. Hävecker, A. Knop-Gericke, L. Schlicker, A. Doran, D. Kober, A. Gurlo et al., *Angew. Chem. Int. Ed.* **2018**, *57*, 14613; *Angew. Chem.* **2018**, *130*, 14823.
[22] N. Köpfle, K. Ploner, P. Lackner, T. Götsch, C. Thurner, E. Carbonio, M. Hävecker, A. Knop-Gericke, L. Schlicker, A. Doran et al., *Catalysts* **2020**, *10*, 1000.
[23] C. Vogt, M. Monai, E. B. Sterk, J. Palle, A. E. M. Melcherts, B. Zijlstra, E. Groeneveld, P. H. Berben, J. M. Boereboom, E. J. M. Hensen et al., *Nat. Commun.* **2019**, *10*, 5330.
[24] K. Han, S. Wang, Q. Liu, F. Wang, *ACS Appl. Nano Mater.* **2021**, *4*, 5340.
[25] J.-H. Kim, D. J. Suh, T.-J. Park, K.-L. Kim, *Appl. Catal. A* **2000**, *197*, 191.
[26] D. Pakhare, J. Spivey, *Chem. Soc. Rev.* **2014**, *43*, 7813.
[27] L. Mayr, N. Köpfle, B. Klötzer, T. Götsch, J. Bernardi, S. Schwarz, T. Keilhauer, M. Armbrüster, S. Penner, *J. Phys. Chem. C* **2016**, *120*, 25395.
[28] S. Cetinkaya, *J. Am. Ceram. Soc.* **2017**, *100*, 5444.
[29] Y. Bleu, V. Barnier, F. Christien, F. Bourquard, A.-S. Loir, F. Garrelie, C. Donnet, *Carbon* **2019**, *155*, 410.
[30] P. Zambaldi, L. Haug, S. Penner, B. Klötzer, *Catalysts* **2022**, *12*, 311.
[31] B. Ølgaard Nielsen, A. C. Luntz, P. M. Holmblad, I. Chorkendorff, *Catal. Lett.* **1995**, *32*, 15.
[32] P. M. Holmblad, J. Wambach, I. Chorkendorff, *J. Chem. Phys.* **1995**, *102*, 8255.
[33] R. Addou, A. Dahal, P. Sutter, M. Batzill, *Appl. Phys. Lett.* **2012**, *100*, 021601.
[34] B. Safavinia, Y. Wang, C. Jiang, C. Roman, P. Darapaneni, J. Larriviere, D. A. Cullen, K. M. Dooley, J. A. Dorman, *ACS Catal.* **2020**, *10*, 4070.
[35] M. A. Vasiliades, P. Djinović, L. F. Davlyatova, A. Pintar, A. M. Efstathiou, *Catal. Today* **2018**, *299*, 201.

Manuscript received: September 7, 2022
Version of record online: November 15, 2022